



Nanofocusing of hard X-ray free electron laser pulses using diamond based Fresnel zone plates

C. David¹, S. Gorelick¹, S. Rutishauser¹, J. Krzywinski², J. Vila-Comamala¹, V. A. Guzenko¹, O. Bunk¹, E. Färm³, M. Ritala³, M. Cammarata², D. M. Fritz², R. Barrett⁴, L. Samoylova⁵, J. Grünert⁵ & H. Sinn⁵

¹Paul Scherrer Institut, CH-5232 Villigen, Switzerland, ²SLAC National Accelerator Laboratory, Menlo Park, CA 94025, USA, ³Department of Chemistry, University of Helsinki, Helsinki FI-00014, Finland, ⁴European Synchrotron Radiation Facility, F-38000 Grenoble, France, ⁵European XFEL, D-22607 Hamburg, Germany.

SUBJECT AREAS:

APPLIED PHYSICS
MATERIALS SCIENCE
NANOTECHNOLOGY
OPTICAL PHYSICS

Received
17 May 2011

Accepted
15 July 2011

Published
8 August 2011

Correspondence and requests for materials should be addressed to C.D. (christian.david@psi.ch)

A growing number of X-ray sources based on the free-electron laser (XFEL) principle are presently under construction or have recently started operation. The intense, ultrashort pulses of these sources will enable new insights in many different fields of science. A key problem is to provide x-ray optical elements capable of collecting the largest possible fraction of the radiation and to focus into the smallest possible focus. As a key step towards this goal, we demonstrate here the first nanofocusing of hard XFEL pulses. We developed diamond based Fresnel zone plates capable of withstanding the full beam of the world's most powerful x-ray laser. Using an imprint technique, we measured the focal spot size, which was limited to 320 nm FWHM by the spectral band width of the source. A peak power density in the focal spot of 4×10^{17} W/cm² was obtained at 70 fs pulse length.

The advent of light sources based on the X-ray free-electron laser (XFEL) principle, has opened the door to a multitude of experiments in various fields of science. The unprecedented brightness, coherence, and the ultra-short pulses of these sources have, e.g., allowed the observation of multiple core-shell ionization and recombination of atoms¹ or coherent diffraction imaging (CDI) with femtosecond exposure to circumvent limitations by radiation damage^{2–4}. Since the Linac Coherent Light Source (LCLS) has recently started to deliver intense XFEL radiation in the hard x-ray range⁵, increasingly challenging experiments can be undertaken such as the ionization of heavier, more complex atoms, or towards CDI of single biomolecules with atomic resolution. In spite of the extreme brightness provided by LCLS, such experiments struggle with poor signal levels. Therefore, it is crucial to compress the hard X-ray beam into the smallest possible focus in order to achieve maximum photon density during a single X-ray shot.

Several nanofocusing schemes have been developed for hard synchrotron radiation. Refractive⁶, reflective⁷, and diffractive⁸ devices can in the best case reach values down to tens of nanometres. So far it has not been possible to focus hard XFEL pulses to comparable dimensions, as this type of radiation imposes more stringent requirements. In particular, due to the much larger transverse coherence lengths at XFEL end stations, focusing optics need to provide typically 10× larger apertures of 0.5–1 mm in order to accept all coherent flux and to concentrate it in the smallest possible (i.e., diffraction-limited) spot. Refractive lenses⁹ with such large diameters provide the short focal length required for high resolution focusing only when stacked in large numbers, making them very lossy. This constraint - as well as strong chromatic aberrations - are the reasons why, so far, only spot sizes of several μm have been produced at XFEL sources. For better resolution and higher efficiency, mirror systems are favoured, but shape errors of the reflecting surfaces on the order of a nanometer are required to sufficiently reduce aberrations. This is why even the most advanced systems are limited by the achievable fabrication and metrology precision, when made large enough to collect the full coherent beam. Foci on the order of 100 nm are targeted¹⁰, however, the performance regarding resolution, wave front quality, and stability still remains to be proven, in situ, under full XFEL radiation load.

The aberrations of diffractive x-ray lenses, i.e. Fresnel zone plates (FZPs), are essentially determined by the placement accuracy of the zone structures. State-of-the-art electron-beam lithography (EBL) tools are capable of writing FZP patterns with negligible distortions¹¹. In consequence, the spot size obtainable under coherent illumination is only limited to approximately the width of the smallest (outermost) zone structures. FZPs can

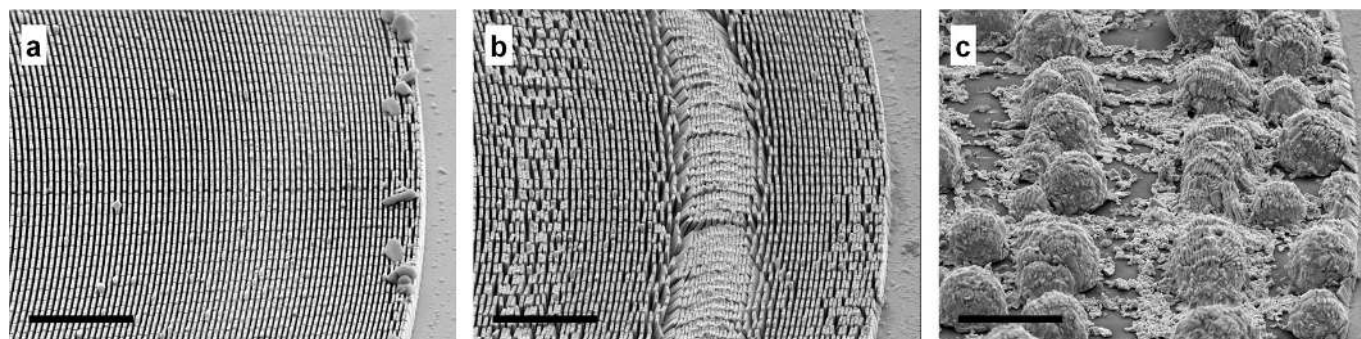


Figure 1 | Gold FZPs damaged by 8 keV LCLS pulses. SEM images of identical devices with 1 μm high structures and an outermost zone width of 100 nm. (a) no irradiation, (b) after 1,000 pulses, (c) after 10,000 pulses. Pulse power: 1.2 mJ, pulse rate: 60 Hz. The scale bars are 4 μm , the view angle is 45°.

be made with large diameters, and the ease of alignment makes them convenient to use. The radiation hardness of such devices consisting of nano-structures placed on thin x-ray transparent membranes has been questioned, and even scenarios to use disposable, single-shot zone plates in XFEL experiments have been considered¹². Recent simulations indicate, however, that the degradation of FZPs in an XFEL beam strongly depends on the materials involved in the manufacturing process¹³. Here we present a first experimental confirmation of these findings.

Results

Three types of FZPs were placed in the full LCLS beam at the maximum pulse energy of approximately 1.2 mJ and a photon energy of 8 keV. The first type of FZPs tested here consisted of gold nano-structures made according to a fabrication procedure frequently applied for devices used at synchrotron end stations (see methods)¹⁴. Several lenses were irradiated, at the maximum pulse rate of 60 Hz and at 10 Hz, and later inspected by scanning electron microscopy (SEM). The image sequence shown in Fig. 1 demonstrates that zone degradation is observed after 1,000 pulses (i.e. after 15 seconds at 60 Hz), and a complete destruction of the FZP has taken place after 10,000 pulses (i.e. within less than 3 minutes). The dose transferred to the Au structures per pulse was approximately 0.1 eV/atom, which is still below the dose required to initiate melting (0.4 eV/atom). However, due to poor heat dissipation, the temperature of the zone structures rises rapidly, triggering recrystallisation of the gold. A comparison with irradiations at 10 Hz pulse rate (see supplementary material B) showed a clear dose rate effect, which confirms, that thermally activated processes play a significant role.

In order to improve the radiation hardness, we developed a fabrication technique for hard X-ray FZPs based on diamond. The excellent thermal conductivity, low X-ray absorption, and high melting point of this material render it ideally suited for this application.

However, diamond is not a material commonly used in nanofabrication. We developed an oxygen plasma etching process to transfer the EBL written FZP pattern into diamond membrane substrates (see methods). The resulting structures are shown in Fig. 2.

Used as an x-ray phase-shifting material at hard photon energies, the main draw-back of diamond is its low refractive index decrement at high photon energies, leading to very low diffraction efficiencies. In order to enhance the number of photons diffracted into the focal spot, diamond zone structures were filled with iridium¹⁵, see Fig. 3a&b by atomic layer deposition (ALD). This approach offers the strong phase-shifting property of this very dense, refractory material (density: 22.5 g/cm³, melting point: 2739 K) in intimate contact with a structure of interdigitated diamond cooling fins for optimised heat dissipation. The gain in focusing power is significant, as shown in Fig. 3c. A pure diamond device was capable of diffracting only 2.1% of the incoming 8 keV radiation into the focus, while the Ir-filled FZP reaches 13.2% efficiency at the same photon energy. Irradiation tests at the XPP instrument confirmed, that the diamond based device did not show any noticeable change in structural integrity or optical performance even after being exposed to $\sim 10^5$ shots of the LCLS, applying the same pulse energy and pulse rate that had destroyed the gold FZPs.

We used the so-called imprint technique to analyse the FZP's focal spot, which has previously been applied to characterise focusing mirrors with spot sizes of several microns at soft XFEL sources^{16,17}. For this purpose, glass slides coated with a thin Au layer were placed into the focal plane of an Ir-filled diamond FZP with 500 μm diameter. We fired a series of single pulses at these samples over a wide range of pulse energies, and analysed the ablated holes generated in the metal coating. The energy was controlled by the beam attenuators of the experimental station. In addition, the random shot-to-shot fluctuations of the XFEL pulse energy were monitored, and used to determine the energy E of each pulse in the focal spot (see methods). When removing all attenuators, we obtain a maximum value of approx. $E_{\text{max}} = 5 \times 10^{-5}$ J.

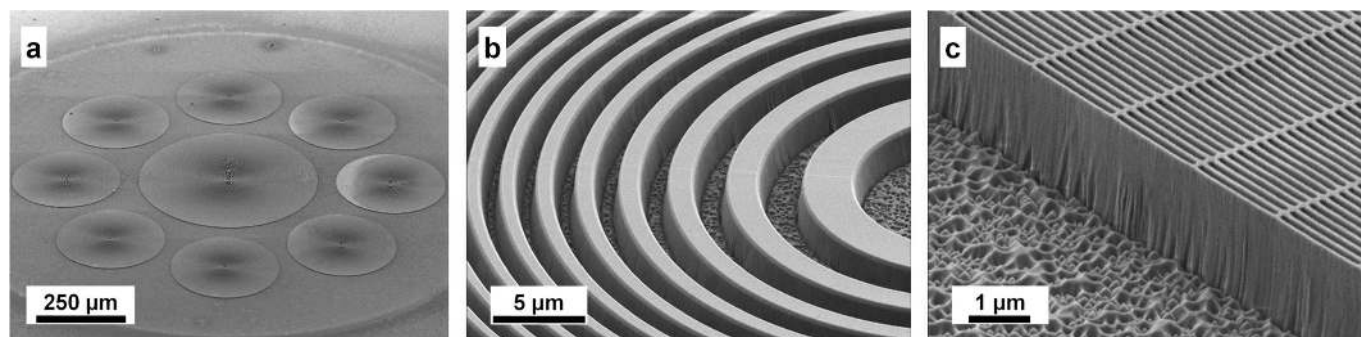


Figure 2 | Diamond Fresnel zone plates. (a) Overview of FZPs etched into a 1.5 mm diameter diamond membrane. The 500 μm diameter of the central FZP is matched to the beam size at the LCLS-XPP end station. (b) Central rings etched 2.1 μm deep. (c) 100 nm wide outermost zones.

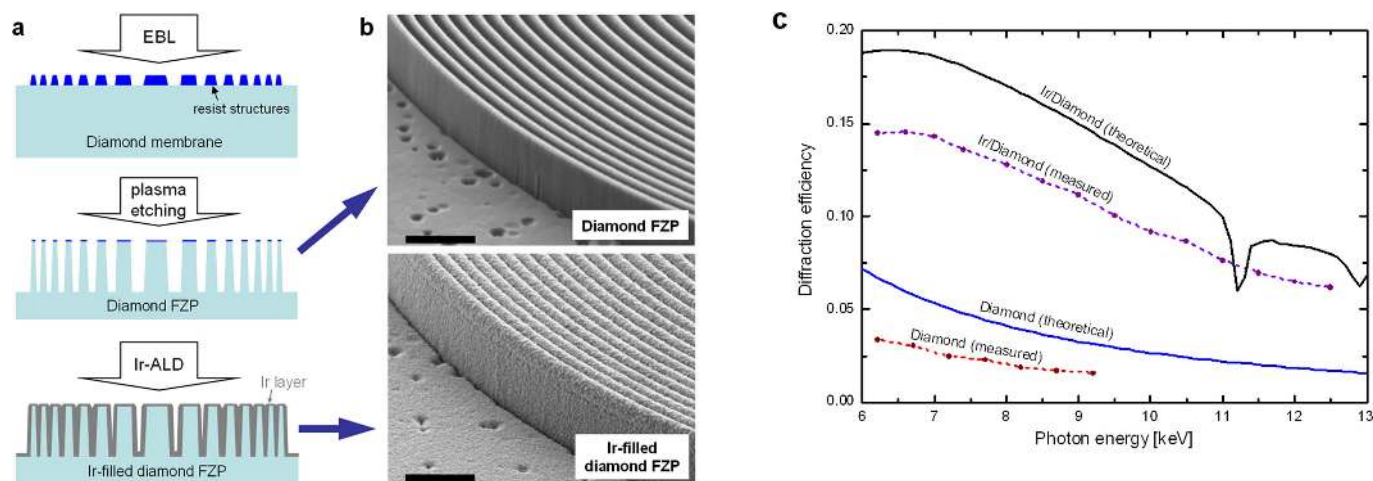


Figure 3 | Improving the diffraction efficiency of diamond-based Fresnel zone plates. (a) Overview of the fabrication flow, comprising electron-beam lithography (EBL) to pattern a resist layer, pattern transfer by plasma etching, and filling with Ir by atomic layer deposition (ALD). (b) Comparison of a diamond test FZP with 1.2 μm high structures and 100 nm wide outermost zones before and after filling with Ir by atomic layer deposition. The scale bars are 1 μm . (c) Photon energy dependent diffraction efficiencies of a diamond FZP with 1.8 μm high structures and a Ir-filled diamond FZP with 1.2 μm high structures. The solid lines show theoretical efficiency of FZPs made from these materials with the corresponding structure dimensions.

Several hundred imprints were analyzed, some examples can be seen in Fig. 4. Following a method introduced by Liu¹⁸, we plotted the squared imprint radius r over the logarithm of the pulse energy E (Fig. 5a). In Liu's model, a Gaussian fluence distribution

$$E(r) = E_0 \cdot e^{-r^2/2\sigma^2} \quad \Leftrightarrow \quad r^2 = 2\sigma^2 \cdot (\ln(E_0) - \ln(E(r)))$$

follows a straight line with a slope of $2\sigma^2$, whereas the x-intercept yields the threshold energy E_0 for ablation of Au. For small fluences our data can be approximated by a line, and a slope corresponding to $\sigma_1 = 120$ nm is found. The intercept at $E_{0,1} = 1.45 \times 10^{-8}$ J can be used to derive a threshold fluence of 7.5 J/cm², corresponding to a dose of 3.2 eV/atom, which is significantly larger than the dose required to bring gold to the boiling point (0.87 eV/atom). This

suggests that most of the absorbed energy is taken away from the thin Au layer and dispersed into the volume of the sample by hot electrons.

At higher fluences, the data shown in Fig. 5a appear to have a linear dependence with $\sigma_2 = 350$ nm. The origin of this second Gaussian is unclear. It could be attributed to long-range interactions in the sample, or indicate spectral components in the vicinity of the XFEL fundamental leading to beam-tails. Nevertheless, the analytical description makes it easy to derive the spot profile in a quantitative way: Fig. 5b shows the same data set of imprints, where the inverse pulse energy is plotted over the imprint radii. Again, the double-Gaussian matches the experimental data well. Its full-width-at-half-maximum (FWHM) value of 320 nm can be taken as the spot

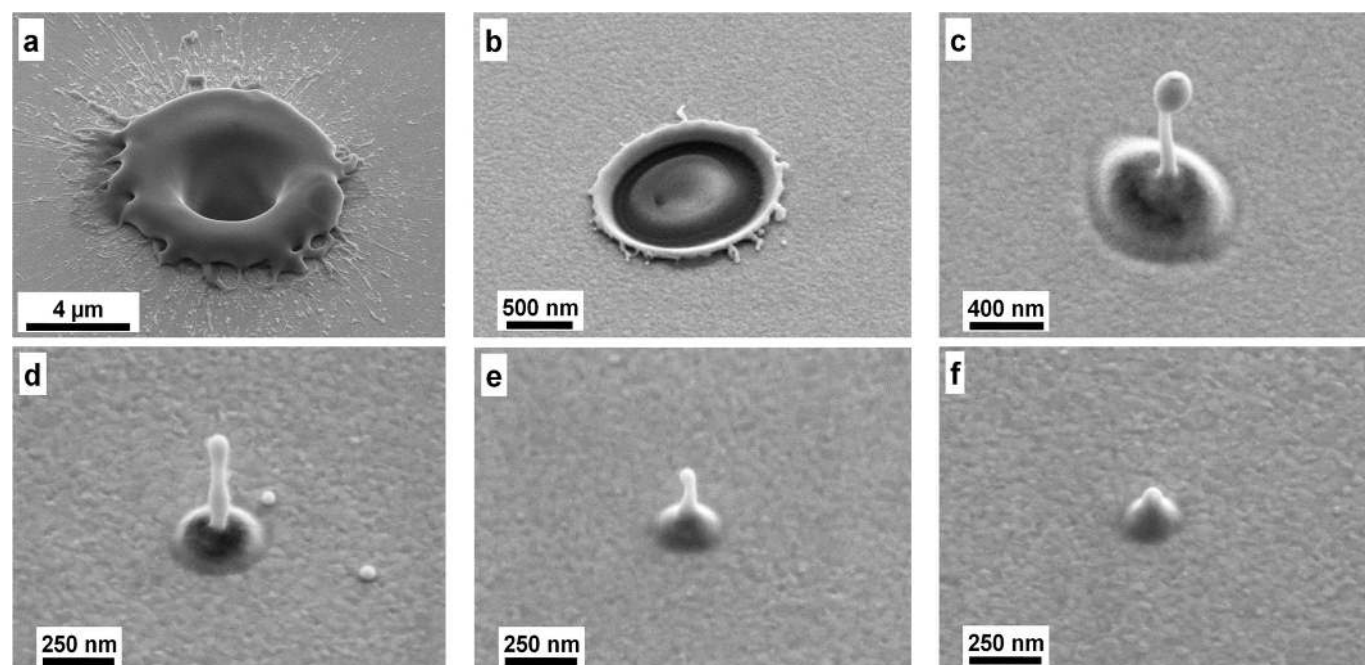


Figure 4 | Imprints created by hard XFEL pulses focused with an Ir-filled diamond FZP. The Au-coated glass substrates are viewed under an angle of 45°. (a) An unattenuated pulse ($\sim 5 \times 10^{-5}$ J) causes a crater with an inner diameter of 3.5 μm . (b, c) Imprints at $\sim 5 \times 10^{-7}$ J and 1×10^{-7} J result in diameters of 1.1 μm and 690 nm, respectively. (d–f) pulses at $\sim 2 \times 10^{-8}$ J result in peak fluences close to the ablation threshold of the Au coating. The imprint diameters are 325, 240, and 190 nm. A fountain of molten glass ejected from the substrate and solidified in the center of imprints c–f.

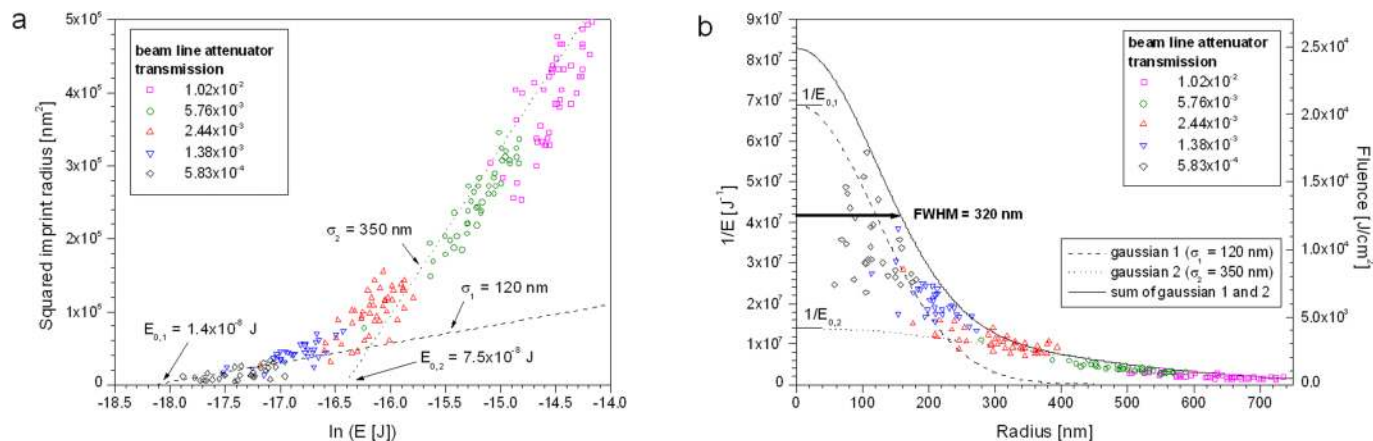


Figure 5 | Analysis of the nanofocus spot size of the Ir-filled diamond FZP. (a) The squared imprint diameters as a function the logarithm of the pulse energy reveals two regions that can be approximated by straight lines corresponding to a double-Gaussian spot with sigma-values of 120 nm and 350 nm, respectively. (b) Beam profile derived from the same data set. The left y-axis shows the inverse pulse energies of the individual shots. The right y-axis is normalised such that the integral energy over the analytical double-Gaussian function is equal to $E_{max} = 5 \times 10^{-5}$ J (see methods).

sizes of our devices. A very similar size and shape was found for the focal spot of a diamond FZP (see supplementary material A).

Knowing the total energy $E_{max} = 5 \times 10^{-5}$ J in the unattenuated focal spot, we can obtain a quantitative fluence profile as shown in Fig. 5b. The right y-axis has been renormalised accordingly, leading to a peak fluence value in the centre of the focal spot of 2.5×10^4 J/cm², that, e.g., created the imprint shown in Fig. 4a. Taking into account a pulse duration of 70 fs (FWHM) results in a peak power densities of approximately 4×10^{17} W/cm². It should be noted, that recent measurements indicate an x-ray pulse duration, which is 2–3 times shorter than the actual electron pulse¹. In this case, the peak power density created in the focus of our lenses would amount to 10^{18} W/cm².

Discussion

We have demonstrated the use of diffractive optics for the nanofocusing of hard XFEL radiation. In contrast to Fresnel zone plates made from conventional materials, the presented diamond-based devices are capable of withstanding the extreme radiation levels at the worlds first hard x-ray laser. The significantly improved heat dissipation through the diamond membrane significantly reduces the temperature during irradiation, effectively suppressing thermally activated damage processes. However, we cannot exclude other damage mechanisms that take place over longer time scales, such as the deposition of hydrocarbons from the residual gas atmosphere. Finite element calculations taking into account scenarios of the future European XFEL indicate¹³, that diamond based devices should provide sufficient heat conductivity to avoid thermally induced damage by this much more powerful XFEL.

The obtained resolution value represents the smallest hard XFEL radiation spot reported to date, and the power density is clearly higher than previously reported from LCLS experiments¹⁹. The gain in photon density provided by the FZP compared to that of the unfocused beam exceeds 10^5 . However, the spot size is significantly larger than the ideal Airy pattern of a zone plate with 100 nm outermost zone width, which should provide a FWHM of 103 nm. The discrepancy can be explained by chromatic aberrations of the FZP at 0.15% relative energy band width, which is close to the value reported for LCLS in Ref. 4 of 0.2%. It can be anticipated, that the performance regarding the achievable spot size will be improved by a factor of 3 through the reduced energy bandwidth of next generation XFELs, that use a seeding scheme²⁰. This would instantly result in an increase of the peak power density by almost an order of magnitude. In addition, the FZPs diffraction efficiency could be significantly

increased to beyond 50% by blazed structures, fabricated either by several layers of aligned lithography steps²¹ or by stacking several FZPs with appropriate geometries²². With such improvements, power densities exceeding 10^{19} W/cm² are within reach. Given these numbers, it can be expected that diamond based diffractive lenses will enable various key experiments at hard XFELs sources.

Methods

Zone plate fabrication. All FZPs used in the experiments described in this letter had 100 nm outermost zone width, and were generated using a 100 keV EBL tool (Vistec EBP 5000Plus). The Au zone plates shown in figure 1 were fabricated on 250 nm thick silicon nitride membranes by electrodeposition of 1 μm thick Au in a mould of poly-methylmethacrylate (PMMA) EBL resist. The fabrication procedure is described in Ref. 14. The diamond based FZPs shown in Fig. 2 were fabricated on polished 4–5 μm thick diamond membranes (Diamond Materials GmbH) supported by Si frames. The membranes were vapour-coated with a 5-nm thick Cr adhesive and conductive layer and then spin-coated with a 400–550 nm thick layer of negative-tone hydrogen silsesquioxane (HSQ) resist (FOX-16 solution, Dow Corning Corp). More details on the fabrication of high aspect ratio FZPs by EBL using HSQ can be found elsewhere²³. The Cr layer was removed by dry etching in a Cl₂/CO₂ plasma to expose the underlying diamond surface. The diamond layers were etched in an inductively coupled plasma reactive ion etcher (Oxford Instruments, PlasmaLab 100). The parameters of the etching are similar to those described in Ref. 24. The ALD of Iridium onto the diamond templates was done using Ir(acac)₃ (acac = 2,4-pentadionato) and O₂ as precursors at 300 °C (F120, ASM Microchemistry Oy). More details can be found in Ref. 15. A layer thickness of 90 nm was deposited, which completely filled the zone structures over the outer 3/4 of the zone plate area.

The efficiency values shown in Fig. 3 were measured at beam line ID06 of the European Synchrotron Radiation Facility (ESRF) in Grenoble, France, according to a procedure described in detail elsewhere¹⁴. The zone plates had 100 μm diameter and were produced according to the procedures described above. The 500 μm diameter FZPs used in the LCLS experiment had similar, but somewhat lower efficiency values at 8 keV photon energy of 7.5% for the Ir-filled device and of 2.0% for the diamond device. This discrepancy can be explained by deviations from the optimum zone profile.

Experimental setup at LCLS. The experiments were performed at the X-ray Pump-Probe instrument (XPP) inside a dedicated experimental chamber evacuated to the 10^{-4} mbar level. It was separated from the beam line vacuum by a 100 μm diamond window. For on-line observation of radiation damage and for alignment, an X-ray camera was placed downstream of the FZP, the imprint samples, and a Be exit window. During all experiments presented here, the LCLS source was operated at 8 keV, 1.2 mJ mean pulse energy, 70 fs pulse length, 250 pC bunch charge, without monochromator. The FZPs chips were clamped to a metal holder without any additional cooling. No central stop or order sorting aperture was used, as the effect of parasitic diffraction orders was negligible.

Radiation damage tests. For each irradiation, a new Au FZP was used and later inspected by SEM. The pulse rate during the irradiation tests on the gold zone plates was 60 Hz for the results shown in Fig. 1. Additional SEM images showing damage induced at 10 Hz pulse rate are shown in the supplementary material B. The level of damage seems to be reduced compared to the 60 Hz irradiation, indicating, that dose rate effects leading to heating of the FZP structures play a dominant role. It is



uncertain whether the Au structures actually reach the melting point, as the extensive deformation and rearrangement of the metal may also occur at somewhat lower temperatures by recrystallization.

Resolution tests. The glass slides were coated with a 5 nm thick adhesive layer of Cr and a 40 nm thick gold layer by thermal evaporation. The slides were placed in the focal plane 323 mm downstream of the FZPs, and series of single pulses were fired at the sample. Attenuators upstream of the FZPs allowed for a control of the pulse power in steps of approximately a factor of 2 (see insets in Fig. 5a and 5b). A finer variation of pulse energy was given by the shot-to-shot fluctuations of the source. The pulse power incident on the FZP plane was determined for each shot by intensity monitors downstream of the attenuators. A beam line transmission of 0.5 was assumed to account for photons lost in the beam line windows and by missing the FZP aperture. Taking into account the measured FZP diffraction efficiency leads to an energy of $E_{max} = 5 \times 10^{-5}$ J in the focus of the Ir-filled FZP when no attenuators are in the beam. This value was used for scaling the x-axis in Fig. 5a and the y-axis in Fig. 5b. However, as the position of the LCLS beam in the FZP plane fluctuated significantly, the fraction of the radiation collected by the FZP aperture varied. This causes a large scatter of the imprint dimensions, which cannot be corrected using the intensity monitor. To account for this effect, the lines in Fig 5a and, correspondingly, the double-Gaussian curve in Fig. 5b were placed such, that they represent envelopes rather than fits of the experimental data. Therefore, only data points close to these lines/curves represent pulses that fully hit the FZP aperture. The imprint diameters in the Au layer were measured in a SEM under normal viewing angle.

1. Young, L. *et al.* Femtosecond electronic response of atoms to ultra-intense X-rays. *Nature* **466**, 56–62 (2010).
2. Neutze, R., Wouts, R., van der Spoel, D., Weckert, E., and Hajdu, J. Potential for biomolecular imaging with femtosecond X-ray pulses. *Nature* **406**, 752–757 (2000).
3. Gaffney, K. J., and Chapman, H. N. Imaging Atomic Structure and Dynamics with Ultrafast X-ray Scattering. *Science* **316**, 1444–1448 (2007).
4. Chapman, H. N. *et al.* Femtosecond diffractive imaging with a soft X-ray free electron laser. *Nature Phys.* **2**, 839–843 (2006).
5. Emma, P. *et al.* First lasing and operation of an ångström-wavelength free-electron laser. *Nature Photon.* **4**, 641–647 (2010).
6. Schroer, C. G. *et al.* Hard x-ray nanoprobe based on refractive x-ray lenses. *Appl. Phys. Lett.* **87**, 124103 (2005).
7. Matsuyama, S. *et al.* Development of scanning x-ray fluorescence microscope with spatial resolution of 30 nm using Kirkpatrick-Baez mirror optics. *Rev. Sci. Instrum.* **77**, 103102 (2006).
8. Vila-Comamala, J. *et al.* Ultra-high resolution zone-doubled diffractive X-ray optics for the multi-keV regime. *Optics Express* **19**, 175–184 (2011).
9. Lengeler, B. *et al.* Refractive x-ray lenses. *J. Phys. D: Appl. Phys.* **38**, A218–A222 (2005).
10. Boutet, S. *et al.* The Coherent X-Ray (CXI) Instrument at the Linac Coherent Light Source (LCLS). *New J. Phys.* **12**, 035024 (2010).
11. Chao, W., Harteneck, B. D., Liddle, J. A., Anderson, E. A., Attwood, D. T. Soft X-ray microscopy at a spatial resolution better than 15 nm. *Nature* **435**, 1210–1213 (2005).
12. Byrd, M. *et al.* Enabling instrumentation and technology for 21st century light sources. *Nucl. Instrum. Meth. Phys. Res. A* **623**, 910–920 (2010).
13. Nilsson, D., Holmberg, A., Sinn, H., Vogt, U. Simulation of heat transfer in zone plate optics irradiated by X-ray free electron laser radiation. *Nucl. Instrum. Meth. A* **621**, 620–626 (2010).

14. Gorelick, S. *et al.* High efficiency Fresnel zone plates for hard X-rays by 100 keV e-beam lithography and electroplating. *J. Synchrotron Rad.* **18**, doi:10.1107/S0909049511002366 (2011).
15. Aaltonen, T. *et al.* Atomic layer deposition of iridium thin films. *J. Electrochem. Soc.* **151**, G489–G492 (2004).
16. Chalupský, J. *et al.* Characteristics of focused soft X-ray free-electron laser beam determined by ablation of organic molecular solids. *Optics Express* **15**, 6036–6043 (2007).
17. Chalupský, J. *et al.* Spot size characterization of focused non-Gaussian X-ray laser beams. *Optics Express* **18**, 27836–27845 (2010).
18. Liu, J. M. Simple technique for measurements of pulsed Gaussian-beam spot sizes. *Optics Letters* **7**, 196–198 (1982).
19. Doumy, G. *et al.* Nonlinear atomic response to intense ultrashort X-ray pulses. *Phys. Rev. Lett.* **106**, 083002 (2011).
20. Feldhaus, J. *et al.* Possible application of X-ray optical elements for reducing the spectral bandwidth of an X-ray SASE FEL. *Opt. Commun.* **140**, 341–352 (1997).
21. DiFabrizio, E. *et al.* High-efficiency multilevel zone plates for keV X-rays. *Nature* **401**, 895–898 (1999).
22. Maser, J. *et al.* Near-field stacking of zone plates in the x-ray range. *Proc. of SPIE* **4783**, 74–81 (2002).
23. Vila-Comamala, J. *et al.* Dense high aspect ratio hydrogen silsesquioxane nanostructures by 100 keV electron beam lithography. *Nanotechnology* **21**, 285305 (2010).
24. Babinec, T. M. *et al.* A diamond nanowire single-photon source. *Nature Nanotechnology* **5**, 195–199 (2010).

Acknowledgements

The authors thank the LCLS machine and experiments teams as well as the XPP staff for their great support. We thank Carsten Detlefs, and Thomas Roth of the European Synchrotron Radiation Facility for assistance during the efficiency measurements. Portions of this research were carried out at the Linac Coherent Light Source (LCLS) at the SLAC National Accelerator Laboratory. LCLS is an Office of Science User Facility operated for the U.S. Department of Energy Office of Science by Stanford University. The research leading to these results has received funding from the European Community's Seventh Framework Programme under grant agreements No. 226716 and No. 212348.

Author contributions

The experiment was conceived by C.D., the diamond based Fresnel zone plates were developed, fabricated, and characterised with synchrotron radiation by S.G., J.V., V.A.G., E.F., M.R. and R.B. The experimental set-up was designed by C.D. and implemented at LCLS by C.D., S.R., M.C. and D.M.F. The measurements at LCLS were performed by C.D., S.R., J.K., O.B. M.C., D.M.F., L.S., J.G., and H.S. The LCLS data were analysed by C.D., S.R. and J.K. The manuscript was written by C.D. and S.G. with discussion and improvements from all authors.

Additional information

Competing financial interests: The authors declare no competing financial interests.

License: This work is licensed under a Creative Commons Attribution-NonCommercial-ShareAlike 3.0 Unported License. To view a copy of this license, visit <http://creativecommons.org/licenses/by-nc-sa/3.0/>

How to cite this article: David, C. *et al.* Nanofocusing of hard X-ray free electron laser pulses using diamond based Fresnel zone plates. *Sci. Rep.* **1**, 57; DOI:10.1038/srep00057 (2011).